Modeling Current Distribution Within Conductors and Between Parallel Conductors in High-Frequency Magnetics

Michael Solomentsev, Alex J. Hanson
University of Texas at Austin
2501 Speedway, Austin, TX 78712, USA
mys432@utexas.edu, ajhanson@utexas.edu

***Abstract*—In both planar and wire-wound transformers, large copper cross-sections and parallel windings are often used to increase conduction area and decrease copper loss. However, at high frequency, current is not guaranteed to spread out maximally over the cross-section of a single conductor or to split evenly between parallel conductors. Finite element analysis (FEA) and SPICE-based systems have been used to analyze current distribution within magnetic components, but these methods are computationally intensive. In this paper, we show that Maxwell's equations, in the high frequency limit, yield a set of linear algebraic equations that are rapidly solvable to yield both the current and magnetic field distribution and hence can be used to predict loss and leakage inductance. Due to its simplicity, this method is easily applied to cases with a one-dimensional or two-dimensional distribution of current. We show that predicted results match both FEA simulations and experimental measurements very accurately for a variety of cases. This paper is accompanied by several software implementations of the method. This method can be used to rapidly analyze high frequency current distribution in transformers and can easily be integrated into numerical optimization algorithms.**

***Index Terms*—High Frequency Transformers, Planar Transformers, Current Sharing, Parallel Windings**

I. Introduction

As switching frequencies have increased into the MHz regime for many power converter applications, magnetic components have emerged as a bottleneck to high efficiency and density, primarily due to core and winding loss. For high-power or high-turns-ratio transformers, large conductor cross-sections or parallel-connected turns are often used to reduce conduction loss. The distribution of current across the cross section of a single conductor or between parallel conductors is determined by resistive effects at low frequencies; the distribution is easy to predict and uniform current distribution for low loss is easy to achieve. At high frequencies, however, current distribution within a conductor or between parallel conductors is determined by magnetic effects and uniform distribution is not guaranteed. The principle phenomenon, that high frequency current crowds toward regions of high H field, is known variously as the skin effect and the proximity effect depending on the scenario. It is important to predict this effect and design to mitigate it.

This material is based upon work supported by the National Science Foundation under Grant No. DGE-1828974 and Enphase Energy.

It is increasingly necessary to consider these effects explicitly. Beyond a few MHz, the practicality of mitigating HF current crowding using litz wire is limited due to cost, thermal constraints, and decreasing efficacy as frequency increases [1]. Moreover, even in cases where conductors are thinner than a skin depth, HF magnetic effects still govern sharing between paralleled conductors, and analysis is necessary.

Analyzing current distribution is relatively straightforward under certain assumptions which are often used and sometimes unstated in textbooks, namely that the primary and secondary currents are in phase or perfectly out of phase and that the *net* current in each layer is known by virtue of their series connections. In such cases, H fields between turns can be readily calculated and the corresponding currents are then known for any ratio of conductor thickness to skin depth [2], [3]. Current distribution in scenarios with conductors in parallel is substantially less straightforward, as the solutions for the H fields and the net currents are coupled. Scenarios with substantial magnetizing current such that primary and secondary currents are neither in phase nor perfectly out of phase are likewise more difficult to analyze, though such analysis has been done [4].

Ensuring current distributes evenly between paralleled turns is becoming increasingly necessary, requiring the use of specialized transformer designs to ensure even distribution [5]–[7]. Note that in [5] and [7], these strategies are used despite operation in the hundreds of kHz, well under the skin depth limit.

Finite element analysis software (FEA) is often used to analyze current distributions in transformers, especially for verifying specific designs [8]–[10]. While very common, FEA software is relatively slow and and difficult to integrate with general-purpose programming languages and circuit simulators, greatly limiting its utility for automated optimization.

One established strategy for predicting current behavior is to extract circuit parameters from the physical structure of the magnetic components, then use a circuit simulator (such as SPICE) to solve [8], [11]–[13]. Predictions of current distribution have been done based on Maxwell's equations, but their general application involves the solution of coupled differential equations which again introduces intuitive and computational barriers [14], [15]. Moreover, many of these approaches are based on Dowell's method and only hold for

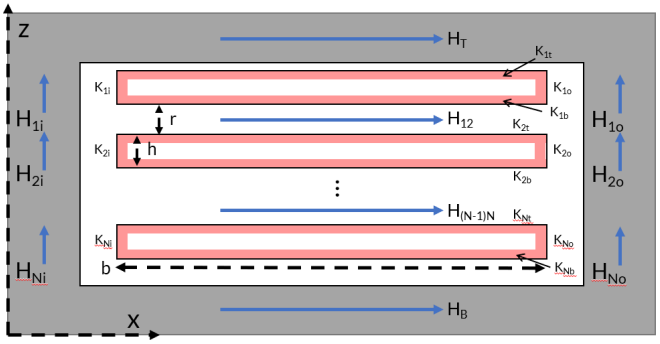

Fig. 1: Notation for the 1-D transformer model, axisymmetric around the Z-axis with turn circumference l.

cases with one-dimensional (1-D) distributions of current [2]. [16] presents a linear application of Maxwell's laws, but is again limited in its applicability (1-D distributions of current, only two parallel conductors, and secondary currents being in phase).

In this work we propose that, in the high frequency limit, Maxwell's equations yield a set of linear *algebraic* equations that fully capture the current distribution in transformer windings. By treating all current flow as surface currents, this approach drastically simplifies the governing equations and accelerates the simulation of current distribution, enabling its integration into automated optimization programs. Furthermore, this approach is also applicable to cases with 2-D distributions of conductors and of current within conductors. Previous work by the authors, presented in [17], restricted this analysis to cases where the transformer was not designed to store energy, and magnetizing current was negligible. The full approach, presented here, applies to any instantaneous current excitation, and thus can be used to estimate current distribution and thus AC resistance in a variety of transformer loading cases. Predicted results match FEA simulations very accurately for a variety of cases. Several planar transformers were built, and show good agreement with our predictions. The contribution of this paper is a computationally lightweight analysis method that can identify current distribution and thus AC resistance and flux distribution in high frequency transformers with high accuracy and at rates several orders of magnitude faster than FEA simulation. The method is singular in its flexibility and breadth of application. Its simplicity and speed enable designers to rapidly test, optimize, and verify transformer designs.

II. Assumptions

To illustrate the problem statement and the proposed approach, consider the transformer cross-section in Fig. 1, which is axisymmetric around its inner axis. A magnetic core surrounds conductive turns which carry current into or out of the page, and may be connected to each other in parallel or in series (each layer is displayed as a single foil layer but may be composed of a spiral of multiple turns and treated as a single foil turn as in [3]).

We make several assumptions about current flow in the transformer. We assume that currents are uniform along each conductor surface. At high frequencies (where the skin depth δ is much smaller than the dimension of interest), the proximity effect causes current to crowd to the surfaces of the conductor; therefore, the current in a layer is modeled as four surface current densities on the top (K_{nT}), bottom (K_{nB}), inner (K_{nI}), and outer (K_{nO}) edges of the layer, each with units of amperes per meter.

This approximation further implies that, in the middle section of the conductor, the current density J, the magnetic field H, and the flux density B are all zero. Because of this assumption, it is not necessary to use Dowell's equations to represent current density in conductors, greatly simplifying the calculation. By *a priori* expecting the current distribution to be spatial impulses (in the z and x dimensions) instead of hyperbolic functions, applying Maxwell's equations to the system results in straightforward algebraic equations, not complicated integrals. This assumption is responsible for the great simplification of the solutions to Maxwell's equations that is at the heart of this approach.

This high-frequency restriction is becoming increasingly applicable for a variety of high-frequency magnetics. Due to manufacturing difficulty, 48 AWG strands are about the thinnest that can be manufactured at a reasonable price, and a great deal of cost-sensitive applications will be economically limited to even thicker strands. The skin depth of copper is equal to the diameter of 48 AWG wire ($31.6\,\mu\text{m}$) at 4.25 MHz. Therefore, as more applications operate in the MHz regime, it will become impractical to simply use extremely thin wires that are smaller than a skin depth (often, several times smaller). This impracticality extends to copper foil which also becomes expensive below 1 mil ($25.4\,\mu\text{m}$) thickness and to planar magnetics on PCBs where the copper thickness offerings are usually limited to 0.5 oz ($17.5\,\mu\text{m}$).

Moreover, balanced current distribution between paralleled turns is not guaranteed at high frequency, even for applications that are not skin depth limited. The proposed method proves accurate in such cases as well, as discussed in Section V.

While Figs. 1 and 5 show axisymmetric structures, this is not an explicit requirement (indeed, the experimental examples in this paper are not axisymmetric and are structured more like Fig. 3). It is also not a requirement that the leakage inductance be zero, or even small; likewise there is no requirement that the magnetizing inductance be very large or that an ungapped structure be used. Indeed, the proposed approach can be used to predict leakage and magnetizing inductances for implementing integrated magnetics in, e.g., dual active bridge or LLC converters.

The approach proposed here also extends to scenarios with 2-D distributions of current that ordinarily would not be solvable with 1-D assumptions (e.g. having a primary and secondary winding in the same layer, as discussed but left unsolved by [12]). Components with a single winding (inductors) can also be analyzed using the general method presented, although these cases are not considered in this work.

In both the 1- and 2-D cases, fields and current densities are treated as being either purely vertical or horizontal - we call this the '1.5-D' assumption. It further implies that conductors are only affected by the magnetic fields in the section of the core directly adjacent to them. In other words, that they

	Type	Sample Equation(s)	# in 1-D Stackup
(A)	Primary & Secondary Current Definitions	$I_P = I_1$ or $I_S = I_2 + I_3$	2
(B)	Total Current in a Conductor	$K_{nT}b + K_{nB}b + K_{nI}h + K_{nO}h - I_n = 0$	N
(C)	Amperian Loop Around Conductor Surfaces	$K_{nB} \pm H_n = 0$ or $K_{nI} \pm \mu_r H_{nI} = 0$	$4N$
(D)	Faraday Loop Between Paralleled Wires	$\frac{1}{2}\delta^2 K_{nB} - \frac{1}{2}\delta^2 K_{mT} + \Sigma\Phi_{enclosed} = 0$	$j \quad (j + k = N - 2)$
(E)	Series Current Connections	$I_1 = I_3$ or $I_1 = I_2 + I_4$	$k \quad (j + k = N - 2)$
(F)	Flux Conservation	$r_n l H_n + \mu_r A_i H_{nI} - \mu_r A_i H_{n+1I} = 0$	$2N + 1$

TABLE I: Equations used in the most general version of the method, with variable b representing conductor breadth, h representing conductor height, l representing conductor length, A_i representing the area of the core inner post, j representing the number of parallel layer interconnections, k representing the number of series layer interconnections (where $j + k = N - 2$), and N representing the total number of conductors.

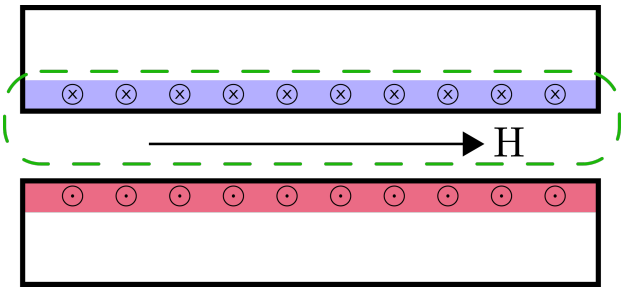

Fig. 2: Diagram of the cross-section of conductors in a 1-D planar transformer, showing in green an amperian loop around a conductor surface described in Section III.

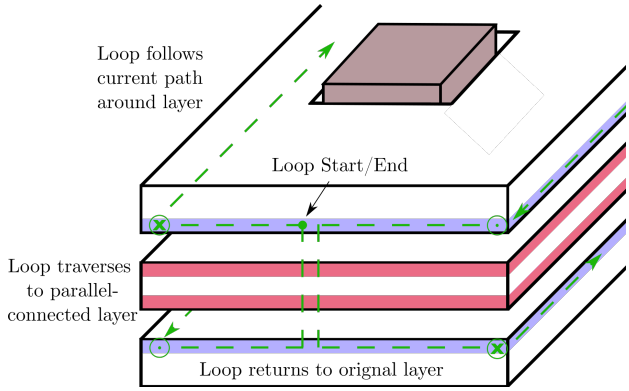

Fig. 3: Labeled diagram of a set of layers in a planar transformer, where the top and bottom layers are connected in parallel. In the method described in Section III, Faraday's Law is applied to the loop shown in green.

are not affected by fringing fields, which can cause current crowding in conductors that are offset from the region of high H field (like a gap) [18]. In practice, this assumption also means that round conductors are modeled as square, with four distinct surface current densities. FEA simulations have confirmed that this simplification results in little loss of accuracy when making current sharing predictions within or between conductors. Further limitations of this assumption are further discussed in Section VI.

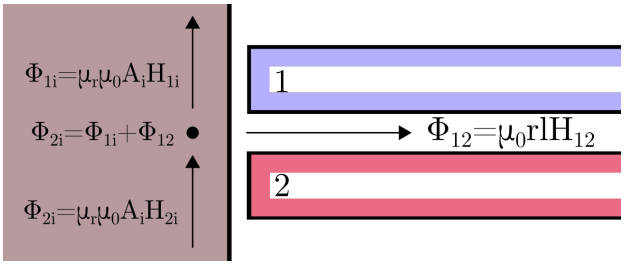

Fig. 4: Labeled diagram showing a set of layer cross-sections and magnetic fields, as an example of applying of Gauss's Law as described in Section III.

III. Analysis Method

A. General Method

Consider a scenario as shown in Fig. 1, with conductors arranged in a single stack as would commonly be the case in a planar transformer. For a system of N conductors, there are $4N$ unknown surface current densities on the top (K_{nT}), bottom (K_{nB}), inner (K_{nI}), and outer (K_{nO}) sides of each conductor. One may also be interested in the corresponding $(N - 1)$ H fields between conductors, the $(2N + 2)$ H fields in the core adjacent to conductor edges, and/or the net currents I_n in each layer. The latter unknowns are easily calculated if the surface current densities are all known, but the presented version of the analysis solves for all $8N + 1$ unknowns. Note that making further simplifying assumptions causes the number of unknowns to be substantially reduced. In particular, assuming net zero ampere-turns in the core (i.e. a situation with no magnetizing current), is of great utility and significance, and will be presented in section III-B.

The analysis method constructs a system of equations based on the structure of the transformer. The resulting solution is true for any instantaneous combination of primary and secondary currents, and can be used to predict current distribution for arbitrary net current waveforms or transformer loading conditions. Readers may want to refer to the equation list in Table I for the remainder of the article. The work is also accompanied on IEEE Xplore by several MATLAB implementations of the analysis method which may be helpful.

First, it is necessary to specify how the primary and secondary currents enter the transformer winding. For example, if it is known that the primary winding begins by entering the transformer on layer one, and the secondary current enters the structure via the parallel connection of layers two and three, we would define these relationships as shown in equation A in Table I. This yields 2 equations. If the primary and secondary currents are not known and depend on the magnetic behavior of the transformer, one may first calculate the leakage and magnetizing inductance using the approach in Sec. III-D and then use these values to predict primary and secondary currents to serve as inputs to this method.

In each layer, the surface current densities sum to the net current in the turn, yielding N equations (see equation B in Table I). Note that because these are surface current densities with units of A/m, the product of a K and a distance indeed yields a result with units of amperes.

Series-connected layers have the same net current, yielding k equations, where k is the number of series interconnections (not series layers) in the structure. (see equation E in Table I). Parallel-connected layers will be considered shortly.

Ampere's Law can be applied by taking loops in the x-z plane around conductor faces, capturing a surface current density and the adjacent H field, either in the core or in the air gaps between conductors (a total of $4N$ equations). This is shown in equation C in Table I, and an illustrative diagram of this loop is shown in Fig. 2. This is equivalent to expressing the electromagnetic boundary condition for H fields, namely that $H_1 - H_2 = K$.

Gauss's law of flux continuity (an example is shown in F in Table I and in Fig. 4) is used in order to relate the H fields at their intersection points. Since winding length l is not necessarily the same for each conductor (for example, in a foil-wound transformer), the system of equations must account for variable l when calculating the H fields and fluxes between conductors. This needs to be applied to every magnetic node except one, chosen arbitrarily. This is similar to the solution of ordinary circuits, in which Kirchoff's current law must be applied to every node except one (usually the exception node is arbitrarily chosen to be ground, whose assignment itself is arbitrary). This produces $(2N + 1)$ equations.

For a structure with only series-connected turns, we have achieved $(8N+1)$ algebraic equations for $(8N+1)$ unknowns and the solution is readily available through matrix inversion.

Parallel-connected turns result in fewer known current equations. For example a pair of series turns results in two equations (each current is known), whereas parallel turns only yield one equation (the *sum* of the currents is known). The loss of these equations is overcome by invoking Faraday's law as an additional constraint (see equation D in Table I), as detailed in [14]. This is relatively simple because the integral of $E \cdot dl$ around each parallel-connected turn must be the same by virtue of the parallel connection. Each loop runs along the surface of the conductor (i.e. where current is non-zero) in a path into and out of the page in Fig. 1, traveling parallel to the direction of current flow in the turns, as shown by the loop in Fig. 3. The derivation is shown below, beginning with the integral form of Faraday's law.

$$\oint E \cdot dl = -\int \frac{dB}{dt} \cdot dA \tag{1}$$

The analyzed loop passes through the surface current densities of both faces, so $E \cdot dl$ is simply the resistive EMF induced along the path.

$$\rho \cdot \Sigma K_{path} = -\omega \cdot \Sigma \Phi_{enclosed} \tag{2}$$

Dividing through by $\omega\mu_0$ gives us a term we can relate to the skin depth, $\delta = \sqrt{2\rho/\omega\mu_0}$.

$$\frac{1}{2}\delta^2 \cdot \Sigma K_{path} + \frac{1}{\mu_0}\Sigma \Phi_{enclosed} = 0 \tag{3}$$

This will yield j equations, where j is the number of parallel interlayer connections (not the number of layers in parallel), where $j + k = N - 2$. Note that we do not express inter-layer fluxes as independent unknowns in the system of equations; rather fluxes are expressed in the form $\mu \times A \times H$, where the relevant permeability and cross-sectional area are known and the H field is the variable of interest (these equations may further be merged with Ampere's law which simply states that the H field and adjacent surface currents K are equal in magnitude). As Faraday's law is taken around full turns of the transformer, the integrals will involve the turn length l. In a scenario such as the one shown in Fig. 1, l will be the same for all windings, although inter-layer distances may vary. In a traditional foil-wound transformer, some conductors are wrapped farther away from the central axis and have a larger circumference, and l will vary for each conductor. For a design with a series-connected primary and a secondary with p turns all connected in parallel, we extract $j = p - 1$ equations. This approach can easily accommodate atypical windings, such as parallel turns in series with another turn.

This method can also accommodate designs with multiple turns in a given layer. When flux is not expected to flow in between the spaces between intra-layer turns, it is possible to simply treat a group of turns as a single conductor with a higher current density. A simple implementation of this can be accomplished by modifying equations (A) and (E) in Table I: If a layer has n series connected turns, equation (A) can be expressed as $\Sigma K = n \times I$, and the $\Phi_{enclosed}$ term in equation (E) is modified to account for the extra current enclosed. In other cases, when flux is expected to flow between intra-layer turns (e.g. when a gap is positioned perpendicular to the layer), the turns may need to be treated as separate conductors, distributed in two dimensions, and analyzed as described in Section III-C.

The resulting system of equations, summarized in Table I, has $8N + 1$ equations and $8N + 1$ unknowns: 2 primary & secondary current definitions; N equations defining total current in a conductor as the sum of its surface current densities; $4N$ Amperian loops around conductor faces; $2N+1$ applications of Gauss's Law; and $N - 2$ Faraday loops around paralleled conductors and series connected conductor current identities (the distribution between these last two types of equations varies depending on the exact structure being analyzed). As such, the analysis method produces a $(8N+1) \times (8N+1)$ square matrix $\boldsymbol{M}$ of coefficients of these equations; a solution vector ($\boldsymbol{x}$) composed of the unknown net currents per layer ($I_1, I_2 \ldots I_N$), the individual surface current densities ($K_{1T}, K_{1B}, K_{1I}, K_{1O}, K_{2T} \ldots K_{NB}$), the H fields between layers ($H_1 \ldots H_N$), and the H fields within the core ($H_{1I} \ldots H_{NO}$); and a known column vector also extracted from the equations above ($\boldsymbol{b}$, where entries are zero except for the total primary and secondary currents). This produces an easily solvable linear matrix equation ($\boldsymbol{Mx} = \boldsymbol{b}$). Note that the $\boldsymbol{M}$ matrix is extremely sparse, and thus the resulting equation is rapidly solvable. We note that the linear matrix equation may be solved through a matrix inversion explicitly, or as is more common (and often faster) in numeric computing, the use of well-known linear algebra solvers. For inclusion in an optimization program, a designer might choose to use an implementation with a limited number of unknowns (e.g. just the surface current densities & H fields) so as not to burden the computation with larger systems of equations than necessary.

There are two cases that can result in even further simplifications – when the primary and secondary currents are in phase or when one of the currents is zero. First, primary and secondary currents are in phase when there are no net ampere-turns in the core (no magnetizing current) – this is a special case where the calculation method can be drastically simplified, as described in section III-B, that applies to transformers in many PWM, series-resonant, dual-active bridge, and other converters. Second, current in one of the windings may be zero for part of the cycle such as in a flyback converter, and the value of the non-zero current can simply be substituted in to the solution vector.

In cases where the primary and secondary current depend on the behavior of the transformer, careful consideration of the loading conditions is necessary. First, the proposed approach can be used to predict magnetizing and leakage inductance (assuming that magnetic impedance dominates the behavior of the transformer, as is expected in high-efficiency structures). The magnetic behavior of the transformer, together with known excitation and loading conditions, can be used to predict the total primary and secondary currents. Finally, it can be noted that the proposed approach yields a time-domain solution, i.e. a solution that is true for any *instantaneous* combination of I_P and I_S. Thus it is possible to apply the proposed solution at a set of sample time points across a period to reconstruct a full solution for individual turn currents, surface current densities, and H fields (which may not be in phase with one or either port current). For sinusoidal excitations and linear loads, unknowns can be expressed as sinusoids with amplitudes and phases by extracting these parameters from the time-domain reconstruction. In addition, while this method is simple to perform with sinusoidal currents to the transformer, it is trivial to input more complex current waveforms as well (e.g. sawtooth or trapezoidal waveforms, commonly found in many converters). If the fundamental waveform frequency is high enough to meet the skin-depth assumptions of the approach, then the harmonics (at higher frequency) will as well. Therefore, we expect the proposed approach to work for arbitrary waveforms (i.e., waveforms with multiple frequency components). This full process can be summarized as follows:

- Use the proposed approach to calculate leakage and magnetizing inductance
- Use the magnetic behavior of the transformer to predict primary and secondary current based on known excitation and known loading (this may be sinusoidal or not; linear or not)
- Use the predicted primary and secondary current in the proposed approach to predict current distribution within conductors, current distribution between parallel conductors, and H fields

Note that this full process is only necessary if the primary and secondary currents can not be treated as known excitations. If the load impedance is significantly larger than the secondary-referred magnetizing impedance, the secondary current will be near zero across an entire period, and a single application of the approach will be sufficient to provide accurate characterization of current distribution and AC resistance. If the load impedance is significantly smaller than the secondary-referred magnetizing impedance and the transformer is excited such that both windings have currents in phase, we suggest the use of the simplified method described in the following section. A decision tree that summarizes how to apply the method is presented in Appendix B.

B. Analysis of Structures with Zero Net Ampere-Turns

In cases where the magnetizing inductance of the transformer is not substantially excited (i.e. the transformer is designed to store minimal energy in the core and the magnetizing current is much smaller than the primary current, implying zero net ampere-turns or $N_1 i_1(t) \approx -N_2 i_2(t)$), the above method can be further simplified. This particular assumption is routinely true in a number of applications: most power transformers for PWM converters, gate-drive transformers, dual active bridge transformers, current transformers, series-resonant transformers, etc. However, in cases where gapped transformers are used to store energy (e.g. in flyback or LLC converters), this assumption will not hold and the more general analysis technique may be necessary.

In zero-ampere-turns cases, we can simplify the problem by assuming that the H fields in the core are negligible. From this, Ampere's Law simplifies for conductor faces adjacent to the core which must be zero. In addition, for many structures (planar structures included) it may no longer be necessary to apply Gauss's law, since the H fields in the core are not relevant. Nevertheless, it would still be necessary to apply Gauss's law when there are magnetic nodes within the core window where different flux paths intersect, as shown in Fig. 5.

For the same scenario described above, a 1-D stack of N conductors, it is now only necessary to consider $3N$ unknowns: N layer currents and $2N$ surface current identities. It is convenient to abstract away H fields for the purpose of more rapid calculation, because they can be readily expressed as linear combinations of the other unknowns. As such, the current identities are unchanged compared to the full method.

The amperian loops are now drawn around adjacent conductor faces, capturing the bottom surface current density of one layer and the top surface current density of the next ($N-1$ equations, see equation C in Table II). However, no net H field is captured when taking this loop (the H field is zero while inside the conductors and the core), so the resulting equation tells us that adjacent current densities must be equal in magnitude and opposite in polarity. This simply replicates the well-known boundary condition for H field parallel to the conductor-air boundary: $|\Delta H| = |K|$, where the H field is shared by adjacent conductors. Amperian loops are also taken around conductor faces which border the core (2 additional equations, for a total of $N+1$ amperian loop equations).

Applying Faraday's law is similar to the general 1-D case. Note that it may be necessary to express inter-layer flux as a linear combination of layer currents and inter-layer cross-sectional areas, calculated using an amperian loop that only crosses the window in one inter-layer space. This is made simple because, by our assumptions, there is negligible H field

	Type	Sample Equation	# in 1-D Stackup
(A)	Primary Current Definition	$I_P = I_1$ or $I_P = I_2 + I_3$	1
(B)	Total Current in a Conductor	$K_{nT}b + K_{nB}b - I_n = 0$	N
(C)	Amperian Loop Around Adjacent Surfaces	$K_{nB}b + K_{(n+1)T}b = 0$	$N+1$
(D)	Faraday Loop Between Paralleled Wires	$\frac{1}{2}\delta^2 K_{nB} - \frac{1}{2}\delta^2 K_{mT} + \Sigma\Phi_{enclosed} = 0$	j
(E)	Series Current Connections	$I_1 = I_3$ or $I_1 = I_2 + I_4$	k

TABLE II: Equations used in the simplified no magnetizing current case, as presented in Section III-B, with variable b as conductor breadth; δ as the skin depth, l as conductor length; j as the number of parallel layer interconnections; k as the number of series layer interconnections (where $j + k = N - 2$); and N as the total number of conductors.

in the core. Thus, the H field between any two windings is simply equal to the sum of currents 'above' or 'below' it (sign-adjusted). For example, if an amperian loop is taken through the core on three sides and around the top two layers in a planar stack, the H, B, and Φ between the second and third layers can be found:

$$\Phi_{23} = rlB_{23} = \mu_0 rlH_{23} = \mu_0 rl(I_1 + I_2) \tag{4}$$

Because the amperian loops taken have assumed zero net ampere-turns in the core, they imply that the secondary current must be the negative of the turns-ratio-adjusted primary current. As such, there is no need to specify the secondary current explicitly, and only one current definition is needed (equation A in Table II).

The final system of equations has $3N$ equations and $3N$ unknowns, a marked decrease in complexity from the full method outlined above. It is possible to decrease the matrix size further by expressing everything in terms of current densities and eliminating the outermost current densities (which are always zero, based on these assumptions). We retain the total layer currents and all surface current densities for purpose of clarity. For many applications, it may be most appropriate to use this method, especially when integrated into optimization engines. Note that Section V and Fig. 13 show the full system of equations and corresponding matrix respectively for an application of this method to an eight layer planar transformer. In addition this work is accompanied on IEEE Xplore by several MATLAB implementations of the method.

Compare this to the method presented in [15], where a linear matrix equation is also constructed, but its coefficients must be extracted from several other systems of equations involving second order differential equations and hyperbolic functions. In contrast, the method presented in this paper is entirely algebraic and significantly more straightforward. Both symbolic and numerical solutions for transformers with many layers can be computed extremely quickly. Moreover, the solution yields a great deal of information about the transformer, including the values of the H fields, the current carried in each layer, and the current distribution between the multiple 'skins' on each conductor. The primary restriction here is the assumption that the transformer is "skin-depth-limited," i.e. that the frequency of operation is high enough to force currents to flow in distinct skins on conductor surfaces. This is neither an unusual situation nor as restrictive as it may seem for predicting current sharing in parallel layers (see Section V).

C. Analysis of Structures with 2-D Distribution of Conductors

The above method is described for a structure with a 1-D distribution of conductors, i.e. planar or foil wound transformers. However, it extends straightforwardly to structures with a 2-D distribution of conductors, as shown in Fig. 5. The same equations are used, and the '1.5-D' assumption (that the H fields are entirely vertical or horizontal) already present in the general method figures prominently in 2-D problems. Analysis of these structures was previously limited to FEA software; the authors are unaware of any existing analytic approach in these cases.

Choosing loops on which to apply Faraday's law is slightly more complex in the 2-D case, because parallel-connected turns may sit in different columns and/or rows. This simply requires us to account for the flux flowing through the loop in both the x and z dimensions. For example, in Fig. 7b, turns 2 and 3 (the top conductor of the outer column, and the middle conductor of the inner column, respectively) are in parallel. To accurately apply Faraday's law, we draw a loop running through K_{2I} and K_{3T} (labeled on the figure), and sum the flux flowing through this loop, either H_{13} and H_{12}, or H_{24} and H_{34}. We then construct a linear matrix equation and solve as in the 1-D case.

While this extension is more general, it is not always necessary. When columns or rows consist of a series connection of turns, they can often be grouped and treated as a single foil turn [3], and the 1-D assumption is more straightforward and yields accurate results for the one dimension considered. Nevertheless, even in these cases the H field between series-connected turns and the corresponding surface currents may be of interest and the 2-D calculation approach is required to solve for them. In both the 1-D and 2-D models, many of the equations are extremely simple, and can be simplified further. Much like the 1-D case, the resulting system is entirely composed of linear, algebraic equations, and can be assembled into a sparse matrix which has very low computational burden.

D. Calculation of Leakage Inductance

Leakage inductance can be readily calculated with this solution and the dimensions of the transformer. By applying a thought experiment in which the primary and secondary are excited by opposite and turns-ratio-adjusted current sources, the total energy storage in the transformer is attributable to leakage inductance, as the magnetizing inductance is not excited. Although we apply a thought experiment that matches

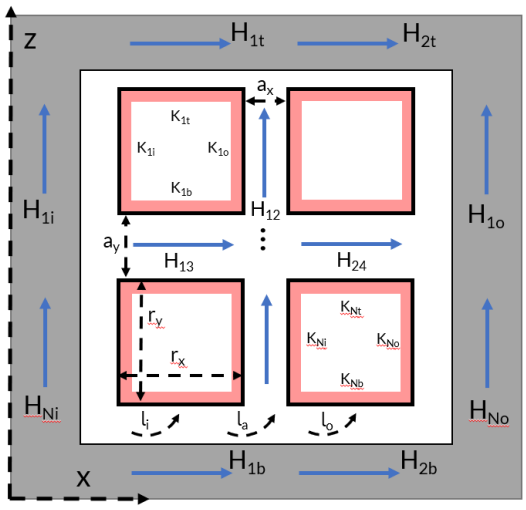

Fig. 5: Notation for the 2-D transformer model, axisymmetric around the Z-axis with inner turn circumference l_i and outer turn circumference l_o.

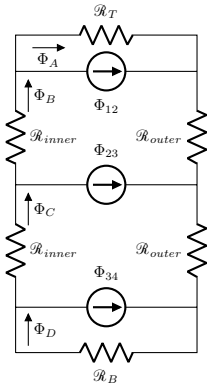

Fig. 6: Magnetic circuit model of a four-layer transformer with pre-solved inter-layer fluxes used to calculate leakage inductance.

the zero-net-ampere-turn assumption, it is not necessary for the intended application to fit this assumption, as leakage inductance is a property of the transformer independent of its application. Computing the result when the transformer is excited in this way, the total leakage energy can be found as $W_{lk} = \frac{1}{2}\mu_0 \int H^2 \cdot dV$, yielding the sum of the leakage inductances as viewed from the primary $L_{lk,pri} = W_{lk}/I_{pri}^2$ or the secondary $L_{lk,sec} = W_{lk}/I_{sec}^2 = W_{lk}/I_{pri}^2 \times (N_2/N_1)^2$. If it is important to distinguish between primary leakage L_{l1} and secondary leakage L_{l2} as commonly defined in the T model of the transformer [19], the designer can convert the calculated H field values to their corresponding fluxes, then build a magnetic circuit model (an example for a four-layer transformer is shown in Fig. 6) using the known interlayer fluxes as sources (Φ_{12}, etc.) and core reluctances based on the transformer structure. The magnetic circuit can be solved and the flux linkage λ in each winding can be determined by summing the fluxes that penetrate the turns/layers that correspond to that winding, and the leakage inductance is found by dividing by current, e.g., $L_{l1} = \lambda_{pri}/i_{pri}$, where λ_{pri} is the flux linkage for the primary winding and i_{pri} is current in the primary winding.

IV. Comparison to FEA Simulation

A. Zero Ampere Turns Case

We begin by demonstrating the validity of the approach presented in III-B as it is a specific simplification of the general approach. Due to its lighter computational load and broad applicability, it may be more suitable for many applications. We compare its predictions to those of FEA simulation for several example cases. We simulated several transformers with six conductors arranged in 1- and 2-D configurations at 300 kHz (resulting in a skin depth much smaller than the conductor thickness) in ANSYS Maxwell, an FEA solver. We extract the current in each conductor, and analyze the same structures using the presented method. Results from one 1-D and two 2-D six-conductor transformers are presented in Table III. We use the notation $a/b/c/\ldots$ to indicate how current divides between parallel layers, where a,b,c, etc. are given as decimals whose sum is unity.

In the 1-D, 6-layer model (Fig. 7a), solving the system of equations from Table II predicts current to split .5/.333/.167 between layers 2, 4, and 6 when those layers are paralleled as secondary windings. FEA simulation produces the same results. The model also has good matching in cases with more complex winding arrangements, for example the 8-layer winding shown in Fig. 7d where the secondary consists of layer 5 connected in series with layers 2 and 6 connected in parallel. The analysis method predicts that if the primary is excited with 1 A, layers 2, 5, and 6 should have currents with peak magnitudes of 1.624, 2.5, and 0.874 A flowing through them respectively. FEA predicts 1.624, 2.498, and 0.874 through layers 2, 5, and 6 respectively, indicating very strong agreement between the model and FEA simulation.

FEA simulations also align closely with our predictions for 2-D models. In both 4- and 6- wire configurations with paralleled turns in different columns, the predicted current sharing ratio is consistently within 1% of the simulated value. Table III shows predictions and simulated data from two 2-D simulations, one where parallel turns are alternated between columns, and one where they are crowded at the top of the structure. In both cases, the algebraic matrix equation of Table III yields results with excellent agreement with FEA simulations. Moreover, the proposed method predicts surface current densities well, indicating which sides of conductors are subject to the most current crowding. This is slightly more difficult to quantify while accounting for the conductor corners, which are shared by two surfaces, but can be qualitatively validated by inspecting FEA outputs, as shown in Fig. 7. For example, for the structure shown in Fig. 7c, the proposed approach

Design	Method	I_{p1}	I_{p2}	I_{p3}
1D; 2/4/6 Paralleled	Model	50.0%	33.3%	16.7%
	FEA	50.0%	33.3%	16.7%
2D; 2/3/6 Paralleled	Model	24.0%	52.0%	24.0%
	FEA	23.8%	52.4%	23.8%
2D; 1/2/3 Paralleled	Model	0.0%	22.1%	77.9%
	FEA	1.4%	22.4%	76.2%

TABLE III: Predicted and FEA simulated current sharing ratios for several transformer structures, showing close agreement between the two.

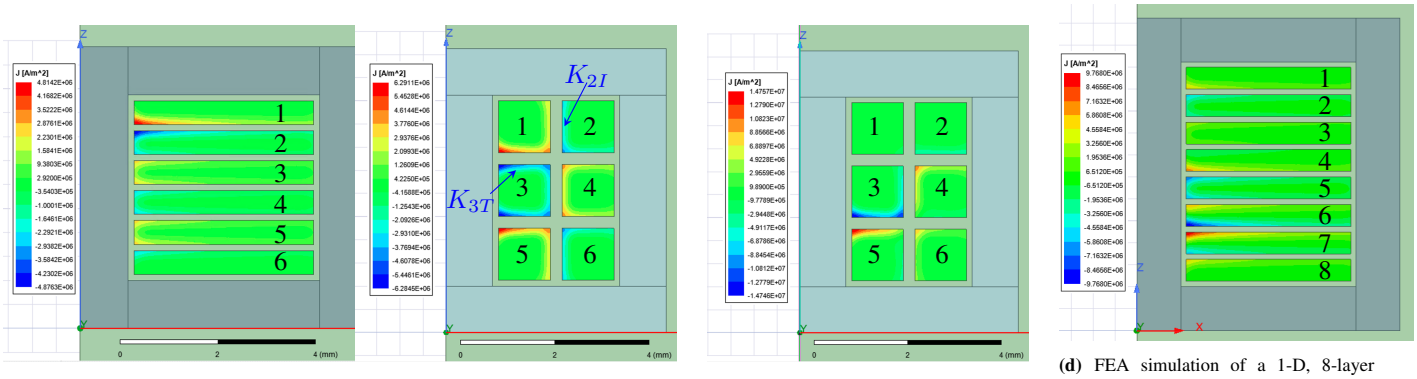

(a) FEA simulation of a 1-D, 6-layer transformer with layers 2, 4, and 6 as a parallel-connected secondary

(b) FEA simulation of a 2-D, 6-turn transformer with turns 2, 3, and 6 as a parallel-connected secondary

(c) FEA simulation of a 2-D, 6-turn transformer with turns 1, 2, and 3 as a parallel-connected secondary

(d) FEA simulation of a 1-D, 8-layer transformer with a secondary consisting of layer 5 connected in series with layers 2 and 6 connected in parallel.

Fig. 7: ANSYS Maxwell FEA simulations of transformers operating at 300kHz, with J field plotted on conductors, showing current distribution that closely matches predictions. Extracted current sharing ratios and comparison are shown in Table III.

predicts that the second wire in the inner column, should have current densities of 0, 0, 762, and 1413 A/m, starting on the inner (left) face and moving clockwise. Since we assume current distribution solely on the surface, these values will not directly correspond to values extracted from a FEA simulation. However, we observe that this wire seems to have no current traveling along its inner and top faces, and average J of approximately $7 * 10^{-6}$ and $1.4 * 10^{-7}$ $\mathrm{A/m^2}$ on its outer and bottom faces respectively. These current densities, as well as those from other conductors, correspond well to the surface current density predictions.

B. General Method

We proceed by showing similar agreement between FEA and the general form of the proposed approach, for both one- and two-dimensional distributions of conductors. In ANSYS Maxwell, we simulated a foil-wound 3:1 transformer, shown in Fig. 8a, with an interleaved primary (3 turns in series) and secondary (3 turns in parallel). A gap was placed in the center of the core to ensure non-negligible magnetizing current. We also simulated a 2:1 transformer with two dimensional distribution of conductors, shown in Fig. 9a. The upper, inner turn (conductor 1, by our notation) and the lower, outer turn (conductor 4) compose a series connected primary, and the other conductors (2 & 3) compose a parallel connected secondary. Again, a gap is inserted into the structure to ensure the presence of magnetizing current.

Recall from Section III-A that we solve for a solution vector in terms of total primary and secondary currents, then substitute in values for each based on loading conditions and our inductance predictions. We show these results in the time domain, and compare to transient simulations in ANSYS Maxwell. Results can be expressed as amplitude and phase by extracting from the time-domain solution. Figures 8 & 9 show the combined FEA and analytical results for both methods for two different loading conditions, various frequencies, and various kinds of exciting currents (sinusoidal, sawtooth, and square). Note that in both the 1-D 40 Ω load and 2-D 10 Ω load cases, total secondary current is expected to be very small, due to the large load impedance compared to the secondary-referred magnetizing impedance. However, in the 1-D case, the individual layer currents still have significant current flowing through them, while the secondary conductor currents in the 2-D case also decay in magnitude. Furthermore note that currents need not be sinusoidal. Figure 8 shows a case with accurate current distribution predictions where the primary excitation is a sawtooth waveform and Fig. 9 shows a case with a square wave excitation. The proposed method compares very favorably to FEA simulation in these cases. These results indicate the power and robustness of the proposed method.

It may not be necessary to use the full, general method in many cases. Fig. 10 plots the peak amplitude of I_2 in the foil transformer shown in Fig. 8a across a range of loading conditions. FEA and the general version of the proposed method show strong agreement over the entire range of loading conditions. We highlight that the zero ampere turns prediction, which does not account for loading conditions, produces the same result as both FEA simulation and the proposed general method as long as the magnitude of the load impedance is an order of magnitude or more smaller than the secondary referred magnetizing impedance. As discussed, the zero-ampere-turns case can be very useful by directly calculating current amplitudes without time-domain extraction.

V. Experimental Verification

In order to further validate the accuracy of our layer-level current predictions, we built and tested several 1-D planar transformers in which we directly measured layer currents. We used two kinds of set-ups: 1 eight-layer planar transformer with a 4:1 turns ratio inside of a Ferroxcube 4F1 core; and one with several custom transformers composed of one- and two-layer boards connected by bus wire inside a KoolMu 90 core. To ensure accuracy (considering our assumption that the transformer was completely enclosed by the core), tested transformers were designed to be abnormally long, with multiple core pieces taped together to form one extended core (as shown in Fig. 11), similar to those built in [12]. In all tests, a primary winding was excited using an AR 100A400A power amplifier, and current was measured using

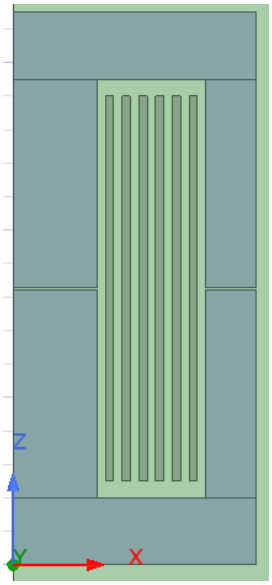

(a) FEA simulation of a 1-D, foil-wound 3:1 transformer. The layers are interleaved, with the innermost layer being a primary turn. The layers are numbered sequentially, with the innermost being layer 1 and the outermost layer 6.

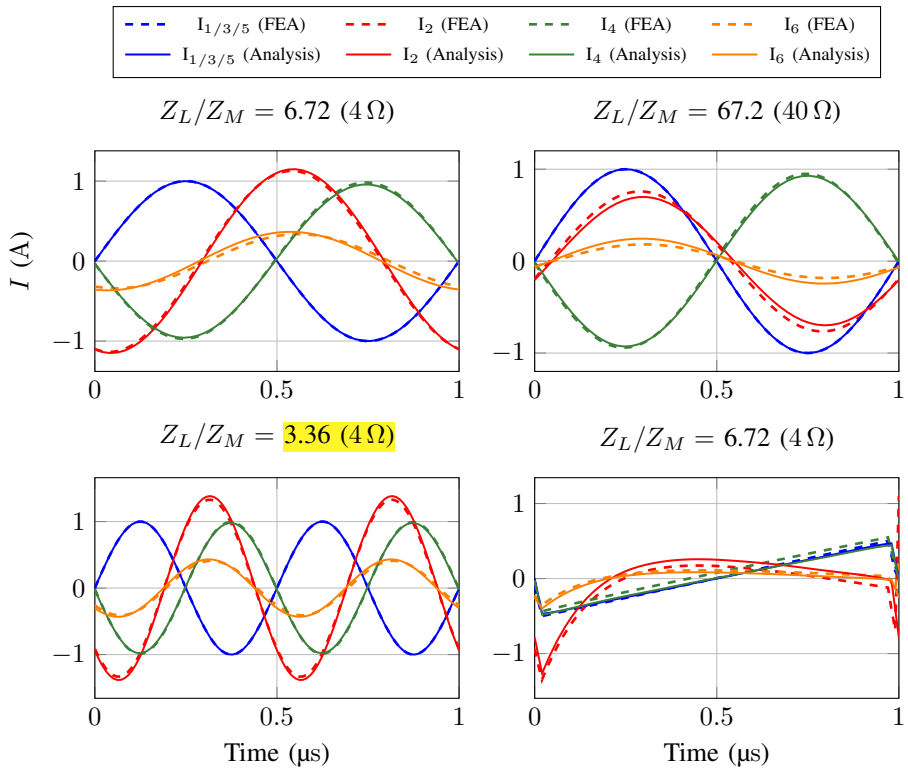

(b) Simulated and predicted current distribution over a period with varying transformer loading conditions, labeled with the ratio of the loading impedance to the secondary referred-magnetizing impedance.

Fig. 8: Comparison of FEA simulated and predicted current for a transformer with 1-D distribution of conductors and magnetizing current operating at 1 and 2 MHz, showing extremely strong agreement.

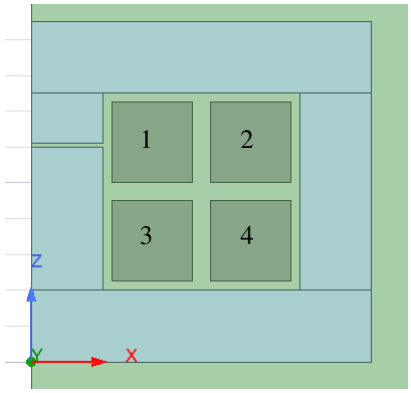

(a) FEA simulation of a 2-D, 4-conductor 2:1 transformer. Conductors are interleaved in two dimensions, with the upper outer turn (2) and the lower inner turn (3) composing the parallel-connected secondary.

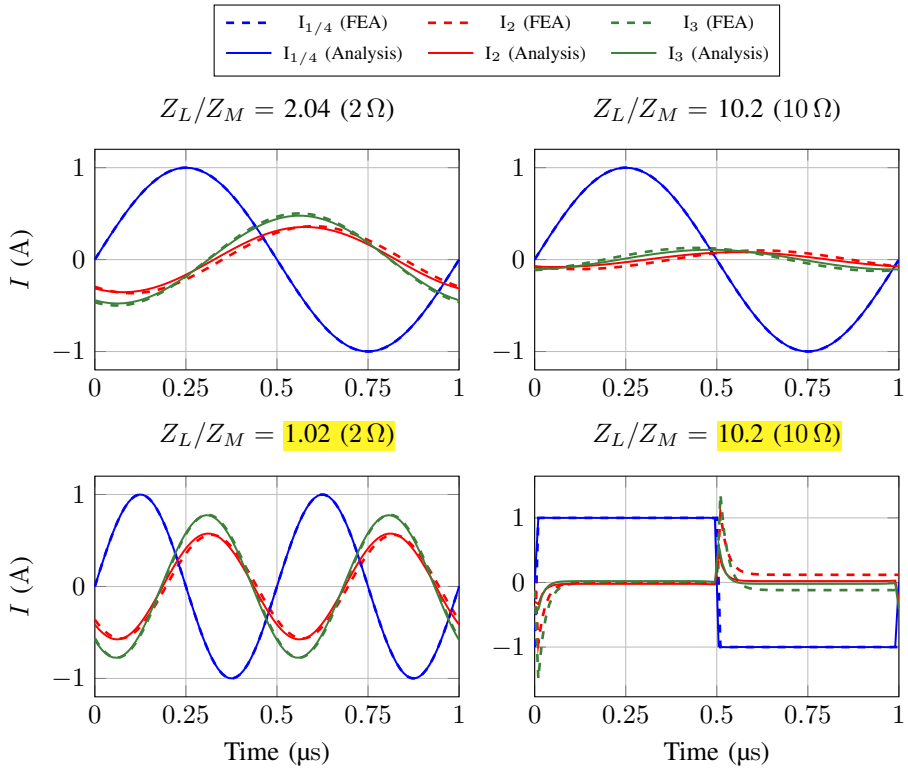

(b) Simulated and predicted current distribution over a period with varying transformer loading conditions, labeled with the ratio of the loading impedance to the secondary referred-magnetizing impedance.

Fig. 9: Comparison of FEA simulated and predicted current for a transformer with 2-D distribution of conductors and magnetizing current operating at 1 and 2 MHz, showing extremely strong agreement.

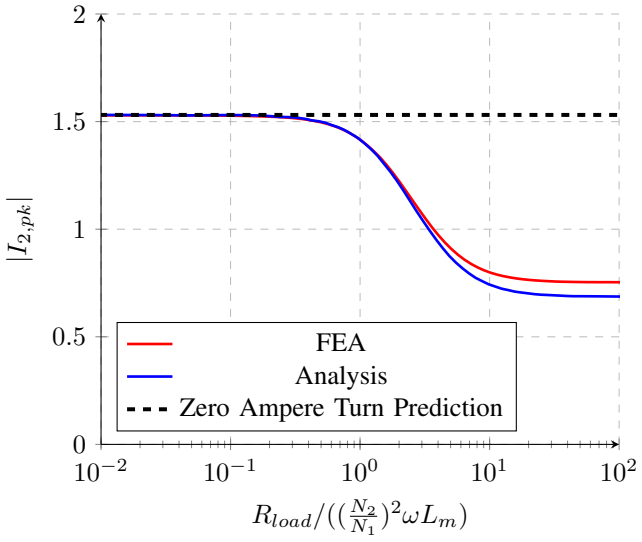

Fig. 10: Plot of predicted $|I_2|$ of the gapped foil-wound transformer shown in Fig. 8a, versus loading condition, showing the applicability of the zero ampere turns method over a large range of loading conditions and the accuracy of the proposed general method.

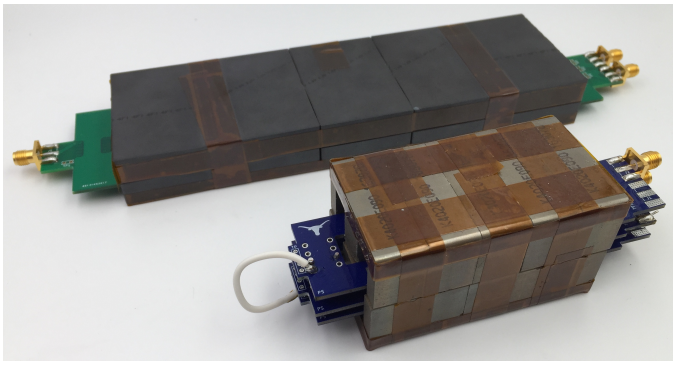

Fig. 11: Experimental set-up, with 8-layer planar transformer in the background, and a stack-up of three 2-layer boards in the foreground

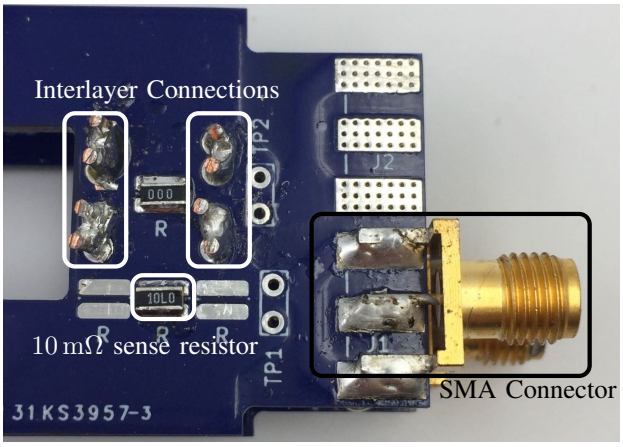

Fig. 12: Close-up of the measurement side of a paralleled secondary layer, showing a SMA connection to a sense resistor

10 mΩ sense resistors on a secondary winding consisting of multiple paralleled layers (see Fig. 12 for a closeup of the measurement set-up on a paralleled layer). Each parallel layer was equipped with its own sense resistor, meaning we could make granular measurements of layer-level current flow at high frequency. All measurements were made with Tektronix IsoVu probes directly connected to the test boards via SMA adapters. In all cases, transformers were excited with sinusoidal currents (and sinusoidal signals were measured by the sense resistors).

The eight-layer board was composed of 1oz copper (approximately 35 µm thick), with layers 2, 3, 4, & 7 as a series-connected primary and layers 1, 5, 6, & 8 as a parallel-connected secondary. The 1.6 mm board had a interlayer spacing of 0.13 mm between layers 3 and 4 and between layers 5 and 6, and a 0.185 mm spacing between all other layers. Using the approach outlined in Section III-B, we predict high frequency current distribution in the structure. We identify 24 unknown layer currents and surface current densities - I_1 through I_8 and K_{1T} through K_{8B}. We then construct a system of equations composed of:

- 1 known primary current identity ($I_2 = I_p$)
- 3 series current relationships ($I_2 = I_3$; $I_3 = I_4$; $I_4 = I_7$)
- 8 summations of current densities to make total layer current ($I_1 = bK_{1T} + bK_{1B}$; $I_2 = bK_{2T} + bK_{2B}$ … $I_8 = bK_{8T} + bK_{8B}$)
- 9 Amperian loops which relate surface current densities in adjacent surface current densities ($K_{1B} = -K_{2T}$; $K_{2B} = -K_{3T}$ … $K_{7B} = -K_{8T}$)
- 3 Faraday loops between parallelled secondaries:

$$
\begin{aligned}
&{}^1\!/\!_{2\delta^2}(K_{1B} - K_{5T}) \\
&\quad = -{}^1\!/\!_{\mu_0}(\Phi_{12} + \Phi_{23} + \Phi_{34} + \Phi_{45}) \\
&\quad = -{}^1\!/\!_{b}(r_1 l H_{12} + r_2 l H_{23} + r_3 l H_{34} + r_4 l H_{45}) \\
&\quad = -{}^l\!/\!_{b}[(r_1 + r_2 + r_3 + r_4) I_1 + (r_2 + r_3 + r_4) I_2 + \\
&\qquad (r_3 + r_4) I_3 + r_4 I_4]
\end{aligned}
$$

$$
{}^1\!/\!_{2\delta^2}(K_{5B} - K_{6T}) = -{}^{r_5 l}\!/\!_{b}(I_1 + I_2 + I_3 + I_4 + I_5)
$$

$$
\begin{aligned}
&{}^1\!/\!_{2\delta^2}(K_{6B} - K_{8T}) \\
&\quad = -{}^{(r_6 + r_7) l}\!/\!_{b}(I_1 + I_2 + I_3 + I_4 + I_5 + I_6) - {}^{r_7 l}\!/\!_{b} I_7
\end{aligned}
$$

These equations are then mapped into a 24x24 matrix and a 24x1 vector shown in Fig. 13. Note that while we have calculated the full symbolic solution (not shown) using MATLAB, it may be more appropriate and faster to calculate a numerical solution depending on the application. Using a MATLAB script running on an AMD Ryzen 3800X, the symbolic solution was produced in 0.3162 seconds, and the numerical solution was produced in $1.515 \cdot 10^{-5}$ seconds. Running on the same computer, an 2D ANSYS Maxwell FEA simulation of an axisymmteric approximation to the same structure ran in 44.5 seconds. When compared to obtaining a single numerical solution (the most equivalent comparison), the proposed method is *over 6 orders of magnitude faster*. This increase in speed is consistent across a variety of cases, since linear systems of equations can be solved very rapidly by computational solvers. FEA approaches may be slower if finer

$$
\begin{bmatrix}
0 & 1 & 0 & 0 & 0 & 0 & 0 & 0 & 0 & 0 & 0 & 0 & 0 & 0 & 0 & 0 & 0 & 0 & 0 & 0 & 0 & 0 & 0 & 0 \\
0 & -1 & 1 & 0 & 0 & 0 & 0 & 0 & 0 & 0 & 0 & 0 & 0 & 0 & 0 & 0 & 0 & 0 & 0 & 0 & 0 & 0 & 0 & 0 \\
0 & 0 & -1 & 1 & 0 & 0 & 0 & 0 & 0 & 0 & 0 & 0 & 0 & 0 & 0 & 0 & 0 & 0 & 0 & 0 & 0 & 0 & 0 & 0 \\
0 & 0 & 0 & -1 & 0 & 0 & 1 & 0 & 0 & 0 & 0 & 0 & 0 & 0 & 0 & 0 & 0 & 0 & 0 & 0 & 0 & 0 & 0 & 0 \\
-1 & 0 & 0 & 0 & 0 & 0 & 0 & b & b & 0 & 0 & 0 & 0 & 0 & 0 & 0 & 0 & 0 & 0 & 0 & 0 & 0 & 0 & 0 \\
0 & -1 & 0 & 0 & 0 & 0 & 0 & 0 & 0 & 0 & b & b & 0 & 0 & 0 & 0 & 0 & 0 & 0 & 0 & 0 & 0 & 0 & 0 \\
0 & 0 & -1 & 0 & 0 & 0 & 0 & 0 & 0 & 0 & 0 & 0 & b & b & 0 & 0 & 0 & 0 & 0 & 0 & 0 & 0 & 0 & 0 \\
0 & 0 & 0 & -1 & 0 & 0 & 0 & 0 & 0 & 0 & 0 & 0 & 0 & 0 & b & b & 0 & 0 & 0 & 0 & 0 & 0 & 0 & 0 \\
0 & 0 & 0 & 0 & -1 & 0 & 0 & 0 & 0 & 0 & 0 & 0 & 0 & 0 & 0 & 0 & b & b & 0 & 0 & 0 & 0 & 0 & 0 \\
0 & 0 & 0 & 0 & 0 & -1 & 0 & 0 & 0 & 0 & 0 & 0 & 0 & 0 & 0 & 0 & 0 & 0 & b & b & 0 & 0 & 0 & 0 \\
0 & 0 & 0 & 0 & 0 & 0 & -1 & 0 & 0 & 0 & 0 & 0 & 0 & 0 & 0 & 0 & 0 & 0 & 0 & 0 & b & b & 0 & 0 \\
0 & 0 & 0 & 0 & 0 & 0 & 0 & -1 & 0 & 0 & 0 & 0 & 0 & 0 & 0 & 0 & 0 & 0 & 0 & 0 & 0 & 0 & b & b \\
0 & 0 & 0 & 0 & 0 & 0 & 0 & 0 & 1 & 0 & 0 & 0 & 0 & 0 & 0 & 0 & 0 & 0 & 0 & 0 & 0 & 0 & 0 & 0 \\
0 & 0 & 0 & 0 & 0 & 0 & 0 & 0 & 0 & 1 & 1 & 0 & 0 & 0 & 0 & 0 & 0 & 0 & 0 & 0 & 0 & 0 & 0 & 0 \\
0 & 0 & 0 & 0 & 0 & 0 & 0 & 0 & 0 & 0 & 0 & 1 & 1 & 0 & 0 & 0 & 0 & 0 & 0 & 0 & 0 & 0 & 0 & 0 \\
0 & 0 & 0 & 0 & 0 & 0 & 0 & 0 & 0 & 0 & 0 & 0 & 0 & 1 & 1 & 0 & 0 & 0 & 0 & 0 & 0 & 0 & 0 & 0 \\
0 & 0 & 0 & 0 & 0 & 0 & 0 & 0 & 0 & 0 & 0 & 0 & 0 & 0 & 0 & 1 & 1 & 0 & 0 & 0 & 0 & 0 & 0 & 0 \\
0 & 0 & 0 & 0 & 0 & 0 & 0 & 0 & 0 & 0 & 0 & 0 & 0 & 0 & 0 & 0 & 0 & 1 & 1 & 0 & 0 & 0 & 0 & 0 \\
0 & 0 & 0 & 0 & 0 & 0 & 0 & 0 & 0 & 0 & 0 & 0 & 0 & 0 & 0 & 0 & 0 & 0 & 0 & 1 & 1 & 0 & 0 & 0 \\
0 & 0 & 0 & 0 & 0 & 0 & 0 & 0 & 0 & 0 & 0 & 0 & 0 & 0 & 0 & 0 & 0 & 0 & 0 & 0 & 0 & 1 & 1 & 0 \\
0 & 0 & 0 & 0 & 0 & 0 & 0 & 0 & 0 & 0 & 0 & 0 & 0 & 0 & 0 & 0 & 0 & 0 & 0 & 0 & 0 & 0 & 0 & 1 \\
\frac{(3r_\alpha+r_\beta)l}{b} & \frac{(2r_\alpha+r_\beta)l}{b} & \frac{(r_\alpha+r_\beta)l}{b} & r_\alpha l/b & 0 & 0 & 0 & 0 & 0 & \frac{1}{2}\delta^2 & 0 & 0 & 0 & 0 & 0 & 0 & -\frac{1}{2}\delta^2 & 0 & 0 & 0 & 0 & 0 & 0 & 0 \\
r_\beta l/b & r_\beta l/b & r_\beta l/b & r_\beta l/b & r_\beta l/b & 0 & 0 & 0 & 0 & 0 & 0 & 0 & 0 & 0 & 0 & 0 & 0 & \frac{1}{2}\delta^2 & -\frac{1}{2}\delta^2 & 0 & 0 & 0 & 0 & 0 \\
2r_\alpha l/b & 2r_\alpha l/b & 2r_\alpha l/b & 2r_\alpha l/b & 2r_\alpha l/b & 2r_\alpha l/b & r_\alpha l/b & 0 & 0 & 0 & 0 & 0 & 0 & 0 & 0 & 0 & 0 & 0 & 0 & \frac{1}{2}\delta^2 & 0 & 0 & -\frac{1}{2}\delta^2 & 0
\end{bmatrix}
\begin{bmatrix} I_1 \\ I_2 \\ I_3 \\ I_4 \\ I_5 \\ I_6 \\ I_7 \\ I_8 \\ K_{1T} \\ K_{1B} \\ K_{2T} \\ K_{2B} \\ K_{3T} \\ K_{3B} \\ K_{4T} \\ K_{4B} \\ K_{5T} \\ K_{5B} \\ K_{6T} \\ K_{6B} \\ K_{7T} \\ K_{7B} \\ K_{8T} \\ K_{8B} \end{bmatrix}
=
\begin{bmatrix} I_p \\ 0 \\ 0 \\ 0 \\ 0 \\ 0 \\ 0 \\ 0 \\ 0 \\ 0 \\ 0 \\ 0 \\ 0 \\ 0 \\ 0 \\ 0 \\ 0 \\ 0 \\ 0 \\ 0 \\ 0 \\ 0 \\ 0 \\ 0 \end{bmatrix}
$$

Fig. 13: Full matrix equation $\boldsymbol{Mx} = \boldsymbol{b}$ for the 8-layer experimental board constructed with the zero ampere turns analytical method. To conserve space, r_α has been used to represent the distance between layers 1 & 2, 2 & 3, 4 & 5, 6 & 7, and 7 & 8, while r_β has been used to represent the distance between layers 3 & 4 and 5 & 6.

meshing or 3D modeling is required. This enormous increase in analysis speed is significant because it allows for integration into automated optimization. [20] describes a software tool that does exactly this - implementing the zero-ampere turns version of the presented method for a simulator and brute-force optimizer of HF planar transformers. The resulting optimizer can process thousands of designs a second, a speed enabled by the lightweight analysis approach presented here.

In the low frequency domain, layer thickness is much smaller than a skin depth and resistive effects dominate how current distributes. There, we expect even current sharing between all parallel-connected layers. At high frequencies, we solve for the unknown vector in Fig. 13. We predict that if the primary is excited with 1A of current, 1.46A, 1.54A, .5A and .5A will flow through layers 1, 5, 6, & 8 respectively. We use the current sharing ratio between the top and bottom layers (both in parallel) as a way to verify the accuracy of our prediction, because these are the only two layers accessible for experimental current measurement. Per our predictions, in the high frequency domain, 2.92 times as much current should flow through layer 1 than layer 8. Experimental results (shown in Fig. 14) validate this, up to transformer self-resonant frequencies.

It should be noted that while the skin depth only becomes equal to copper thickness at approximately 3.5MHz, the high frequency prediction is quite accurate at frequencies as low as 400kHz. This is because the H field in the (much thicker) spaces *between* parallel-connected layers contributes to the mathematics of the magnetic diffusion equation. The approach in this paper does not predict the transition frequency between the low frequency approximation and the high frequency one; as a rule of thumb, identifying where the high frequency approximation prevails for current splitting between parallel layers may be better estimated by comparing the skin depth to the spacing between parallel layers, rather than the thickness of the layers themselves.

Several other planar transformers were built using one- and two-layer boards. These boards were designed to have one turn per layer, and could be configured either in parallel or in series with each other at arbitrary layer spacing using connections of solid bus wire. Moreover, because these are stand-alone boards, the distance between each layer can also be varied. Compare this to the 8-layer board test case, where the inter-layer distance (r_n in our notation) is fixed. When this

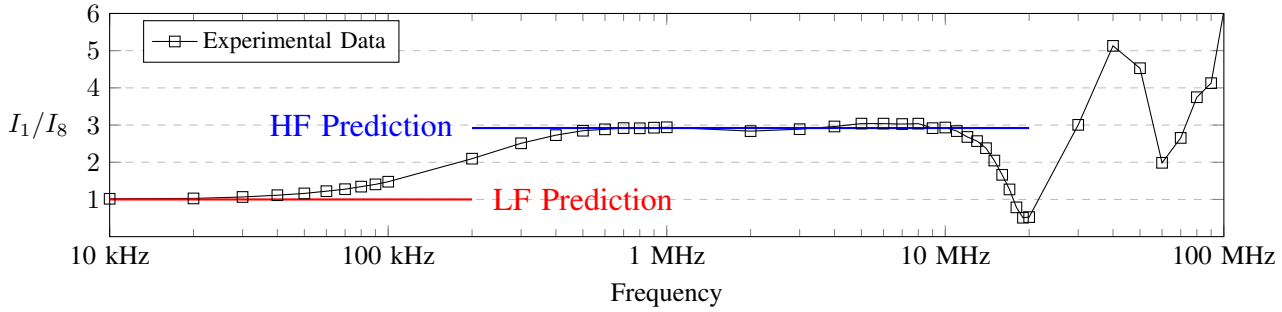

Fig. 14: Experimental current-sharing data from a 8-layer planar transformer with predicted current-sharing ratios overlaid, showing model fidelity at low and high frequency (up to transformer self-resonance).

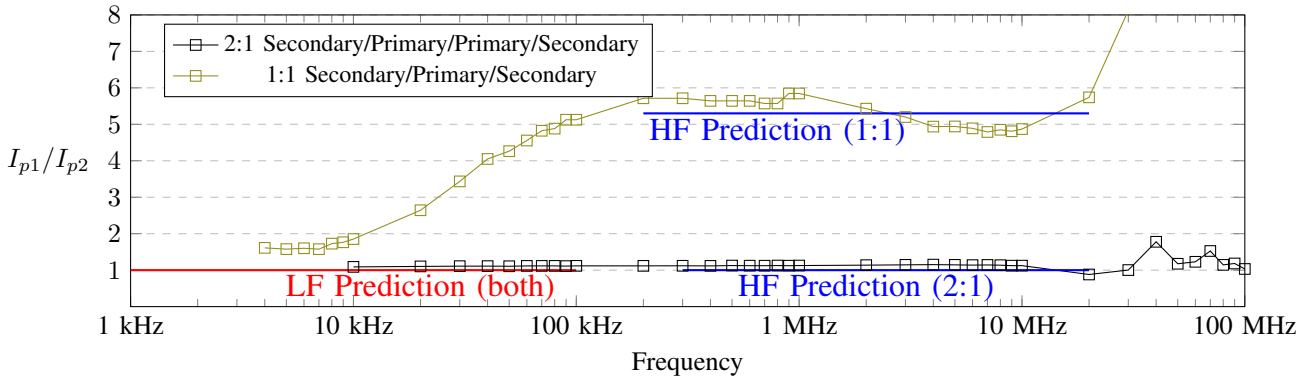

Fig. 15: Experimental current-sharing data from several custom transformers made from several one- and two-layer boards, showing model fidelity at low and high frequency. See the text for details of the transformer structures.

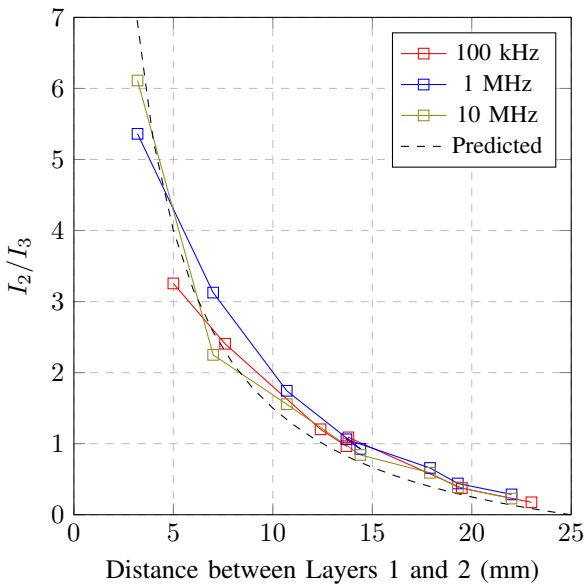

Fig. 16: Current sharing data from a 1:1 Primary/Secondary/Secondary/Primary Transformer, where the distance between layers 1 and 2 (and consequently the distance between layers 3 and 4) is varied to produce different current sharing ratios, showing good agreement with predicted current relationships at various frequencies.

distance is different from layer to layer, this affects the area terms when calculating inter-layer flux (shown in the bottom three equations in Fig. 13. As a result, high frequency current sharing ratios are dependent on the distance between layers.

Fig. 15 shows experimental results from two test cases constructed with the customizable boards (shown in the foreground in Fig. 11). The first is a 2:1 transformer made from four 2 oz copper turns split across two 1.6 mm thick boards. The two paralleled secondary turns sit on the outer two layers, while the series-connected primary turns are on the inner layers. The boards have a turn length of approximately 225 mm, are separated by an 8 mm air gap, and are connected together using bus wire. They are enclosed by five K4020E090 KoolMu cores taped together (shown in Fig. 11). Our analysis predicts that this symmetric structure should experience even current sharing between the two paralleled secondary layers at both low and high frequencies, as shown in Fig. 15.

We predict leakage inductances for the above case, as well as the 8-layer case. For the 8-layer board, when all leakage inductances are referred to the series-connected side: a cartesian FEA simulation predicts 28.4 nH, the energy storage method predicts 29.0 nH, the magnetic circuit method predicts 30.7 nH, and measuring the leakage on the board from the series connected layers using a Keysight E5061B network analyzer yields 53 nH. For the symmetric 4-layer board, when all leakages are referred to the parallel-connected side: a cartesian FEA simulation predicts 17.1 nH, the energy storage method predicts 22.1 nH, the magnetic circuit method predicts 31.7 nH, and measuring the leakage experimentally from the parallel connected layers yields 34 nH. We note that the proposed method fails to reflect all possible leakage paths, considering the 3-D nature of the structure. Despite this, our predictions agree well with with FEA simulations and represent a lower bound on leakage, within a factor of two.

The second test case shown in Fig. 15 is a 1:1 transformer composed of one primary turn interleaved with two paralleled secondary turns, split between two boards (of the same dimensions & composition as those above). The gap between the boards is 8.5 mm. Our prediction indicates that the ratio of between paralleled layers, I_1/I_3, should be equal to r_2/r_1, where r_1 is the distance from layer 1 to 2 and r_2 is the distance from layer 2 to 3. The calculated current sharing ratio is thus $5.3:1$, which matches the experimental data extremely well.

We performed a further experiment on a 1:1 transformer composed of three boards: a two-layer board with paralleled copper turns on either side, sandwiched between one-layer boards connected in parallel with each other. The structure is built such that the inner board can be shifted up and down, changing the inter-layer distance and the current sharing ratio. Based on our analysis, the current sharing ratio between the paralleled secondary layers should be $(\delta^2 + r_3 l)/(\delta^2 + r_1 l)$, which, in the high frequency regime, simplifies to be simply equal to the distance between layers 3 and 4 divided by the distance between layers 1 and 2, or r_3/r_1 in our notation. Fig. 16 shows these measurements at three different frequencies, and shows very strong agreement between experimental results and our model (note that the high frequency prediction prevails even at 100 kHz, where the skin depth of $200\,\mu\text{m}$ is well above the thickness of a layer but still much smaller than any inter-layer spacing).

	This Work	2D FEA	3D FEA	M2SPICE [12]
Simulation Speed (s)	$\sim 10^{-5}$	$\sim 10^{1} - 10^{2}$	$\sim 10^{2} - 10^{4}$	$\sim 10^{-2} - 10^{0}$
Model Complexity	Low	Medium	High	High
Accuracy	High	High	Best	High
Frequency Range	Only HF	No Restriction	No Restriction	No Restriction

TABLE IV: Comparison of the relative advantages of the proposed method and alternative approaches to determining current distribution.

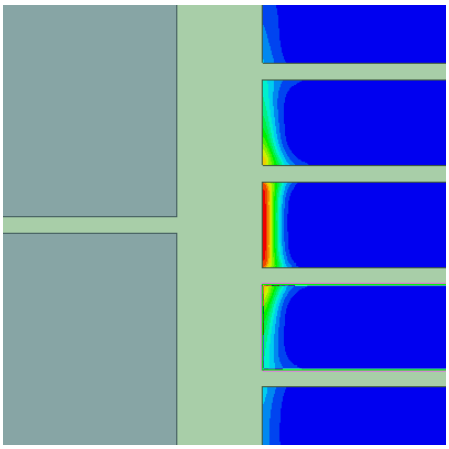

Fig. 17: Close up of a FEA simulation of a planar transformer with a gap inserted into its center post, showing current crowding due to fringing fields that extends to conductors not directly adjacent to the gap.

VI. Limitations

The method presented in this work relies on several simplifying assumptions. While applicable in a wide variety of cases, as detailed in Section IV, these assumptions may not always hold true. Of particular concern is the applicability of the 1.5-D assumption, which enables us to reduce Maxwell's equations to a set of linear algebraic equations.

While the method is capable of predicting current distribution in structures with gapped cores, as shown in Section IV-B, fringing fields around gaps may violate the 1.5-D assumption. Consider, for instance, a planar transformer with a gap inserted in the center post of its core. Depending on the core and gap geometries, the fringing fields may extend far past the boundaries of the gap itself [18]. This in turn, may cause current crowding in conductors not directly adjacent to the gap, as shown in Fig. 17. The proposed method has no way of accounting for these fringing fields, as surface current densities are assumed to be related to the H fields in the segment of the core directly adjacent to them. In the case shown in Fig. 17, the proposed method does not predict current crowding along the inside edge of the conductors directly above and below the gap, leading to general inaccuracy in the full calculation and prediction. Note that this is not a problem for the case where there are zero ampere-turns in the core, as gaps do not cause current crowding when there is not substantial flux in the core.

The 1.5-D assumption also implies uniformity of current density across conductor surfaces, which is not always true. For larger conductors, as shown in Fig. 7, current may still tend to crowd to certain edges of conductors due to the influence of DC resistance effects. While this is unlikely to effect predictions of current distribution between and within conductors (based on our validation of the method), it may contribute to underestimation of AC resistance and loss.

Violations of the 1.5-D assumption may also occur when dealing with structures with extreme aspect ratios. Again, consider the case of a planar transformer. Such a structure might have conductors with total breadths (considering all turns in a layer as a single conductor) on the order of a centimeter or more. These conductors may have typical thicknesses of one or two ounce copper (i.e. $\approx 35\,\mu\mathrm{m}$ or $70\,\mu\mathrm{m}$) and inter-layer spacing in the fractions of millimeters. These small dimensions are not typically an issue when magnetizing current is not considered, as evidenced by strong experimental results with planar transformers. However, when it is important to consider flux through the core (i.e. when magnetizing current is not negligible), the relative dimensions of the structure may prove an issue. For example, consider an ungapped 1:1 transformer with 1 primary turn and 3 turns in parallel on the secondary (with one turn per layer), excited on the primary with an open secondary. Assume that the inter-layer distances, r, are equal to each other, and the layer thicknesses, h, are all equal to each other. The proposed method indicates that changing r and h should cause small variations in the absolute magnitude of the current on each secondary layer, but that the ratios of current distribution should not vary - e.g., when varying r from $0.5\,\mathrm{mm}$ to $10\,\mathrm{mm}$ and h from $0.5\,\mathrm{mm}$ to $5\,\mathrm{mm}$, our prediction of $|I_3|/|I_4|$ remains constant at 0.992. However, when the same structure is simulated using FEA software, and those same parameters are swept, $|I_3|/|I_4|$ varies from 0.182 (when both r and h are $0.5\,\mathrm{mm}$) to .951 (when both r and h are at their maximum values). These results are shown in Fig. 18. We observe a much stronger dependence on the value of r than of h. This indicates that the 1.5-D assumption potentially breaks down as interlayer distances become very small – our assumptions about flux being totally enclosed in the core and branching off at defined nodes are not necessarily accurate. We emphasize, however, that the PCB structures analyzed in Section IV all showcased the accuracy of the proposed method in the zero ampere-turns domain, despite extreme aspect ratios.

VII. Conclusion

Many high-frequency power converters rely on magnetic components of various constructions, including planar, wire-wound, and foil-wound, for voltage conversion, energy storage, and isolation. The detailed distribution of current in conductors is important to calculate to understand ac losses. In addition, paralleling turns may be necessary to minimize loss, especially in cases with high turns ratios, and predicting current sharing between parallel turns is equally important. We have presented a generalizable method for predicting current distribution in these cases that is easily applied and rapidly solved. The relative advantages of this new method, compared to typical commercially available alternatives and prior academic work, is shown in Table IV. The method achieves

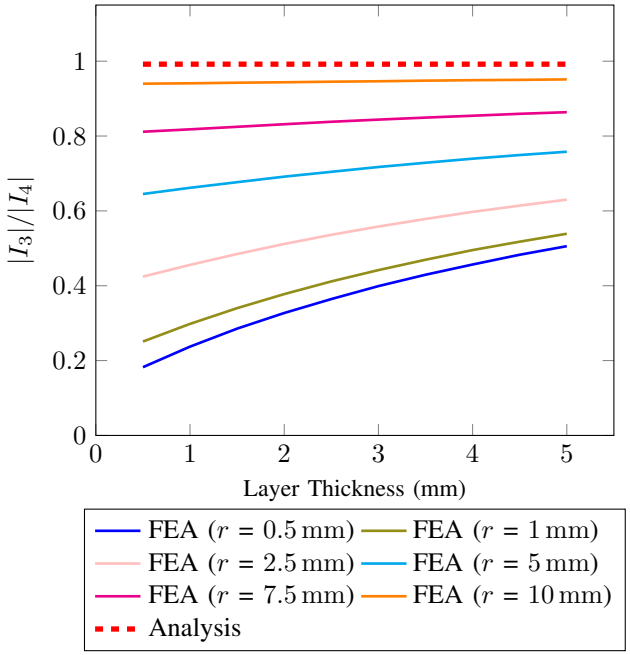

Fig. 18: Comparison of predicted relative current distribution between paralleled layers in 1:1 transformer with varying layer thickness (t) and layer spacing (r), showing greater inaccuracy in the proposed method as interlayer spacing becomes small.

these benefits by virtue of the high-frequency assumption in which currents are assumed to flow only as surface currents on the edges of conductors. This yields a set of linear algebraic equations which is uniquely fast to solve numerically and integrate into optimization algorithms. The simplicity of the approach allows it to extend to cases where the current and magnetic field distributions may be significant in two dimensions; we are unaware of prior approaches that extend to 2-D distributions. Its algebraic nature enables it to be extremely rapid – orders of magnitude faster than FEA simulation. Both FEA simulations and experimental results validate the accuracy of our predictions at a large range of frequencies and for many different structures. Due to its simplicity, such a method can be easily integrated into optimization engines for transformer layer arrangements, and can facilitate the design of low loss high frequency transformers.

Appendix A
Experimental Dimensions

8-Layer Board	
Board Thickness	1.6mm
Copper Thickness	1 oz (35 µm)
Turn Length	46 cm
Turn Width	2 cm
Layer Spacing	0.185 mm, 0.13 mm
Customizable Boards	
Board Thickness	1.6mm
Copper Thickness	2 oz (70 µm)
Turn Length	22.5 cm
Turn Width	9 mm

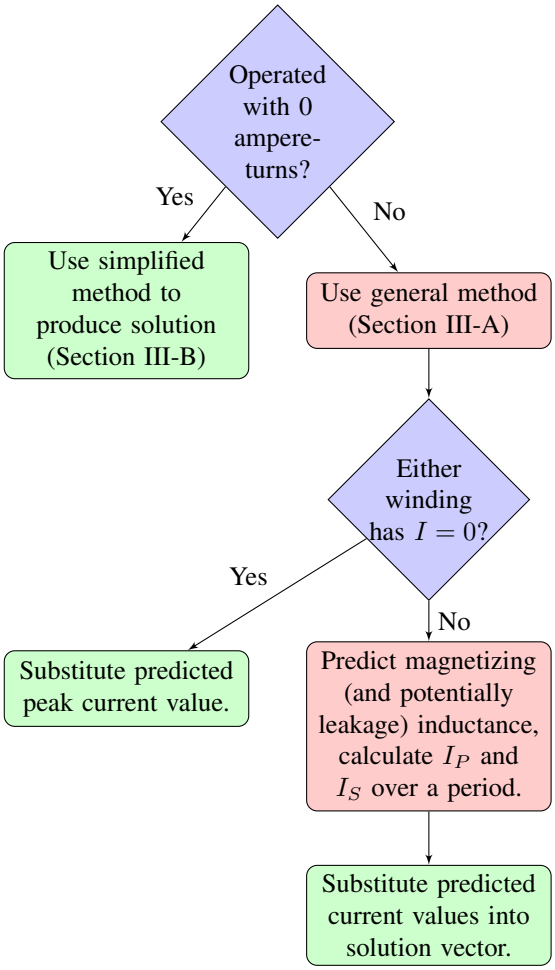

Fig. 19: Decision tree for selecting the most suitable analysis method.

Appendix B
Method Choice Decision Tree

To assist in the selection of the most appropriate version of the analysis method presented for a particular application, refer to the decision tree shown in Fig. 19.

References

[1] C. R. Sullivan, "Prospects for advances in power magnetics," in *CIPS 2016; 9th International Conference on Integrated Power Electronics Systems*, 2016, pp. 1–9.

[2] P. L. Dowell, "Effects of eddy currents in transformer windings," *Proceedings of the Institution of Electrical Engineers*, vol. 113, no. 8, pp. 1387–1394, 1966.

[3] Erickson, Robert W. and Dragan Maksimović, *Fundamentals of Power Electronics*. Springer, 2001.

[4] J. P. Vandelac and P. Ziogas, "A novel approach for minimizing high frequency transformer copper losses," in *1987 IEEE Power Electronics Specialists Conference*, 1987, pp. 355–367.

[5] S. Wang, H. Wu, F. C. Lee, and Q. Li, "Integrated matrix transformer with optimized pcb winding for high-efficiency high-power-density llc resonant converter," in *2019 IEEE Energy Conversion Congress and Exposition (ECCE)*, 2019, pp. 6621–6627.

[6] S. Wang, M. de Rooij, W. Odendaal, J. van Wyk, and D. Boroyevich, "Reduction of high-frequency conduction losses using a planar litz structure," *IEEE Transactions on Power Electronics*, vol. 20, no. 2, pp. 261–267, 2005.

[7] R. Yu, T. Chen, P. Liu, and A. Q. Huang, "A 3-d winding structure for planar transformers and its applications to llc resonant converters," *IEEE Journal of Emerging and Selected Topics in Power Electronics*, vol. 9, no. 5, pp. 6232–6247, 2021.

[8] R. Asensi, R. Prieto, and J. A. Cobos, "Automatized connection of the layers of planar transformers with parallel windings to improve the component behavior," in *2012 Twenty-Seventh Annual IEEE Applied Power Electronics Conference and Exposition (APEC)*, 2012, pp. 1778–1782.

[9] D. Fu, F. C. Lee, and S. Wang, "Investigation on transformer design of high frequency high efficiency dc-dc converters," in *2010 Twenty-Fifth Annual IEEE Applied Power Electronics Conference and Exposition (APEC)*, 2010, pp. 940–947.

[10] Z. Ouyang, O. C. Thomsen, and M. A. E. Andersen, "Optimal design and tradeoff analysis of planar transformer in high-power dc–dc converters," *IEEE Transactions on Industrial Electronics*, vol. 59, no. 7, pp. 2800–2810, 2012.

[11] X. Margueron, A. Besri, Y. Lembeye, and J. Keradec, "Current sharing between parallel turns of a planar transformer: Prediction and improvement using a circuit simulation software," *IEEE Transactions on Industry Applications*, vol. 46, no. 3, pp. 1064–1071, 2010.

[12] M. Chen, M. Araghchini, K. K. Afridi, J. H. Lang, C. R. Sullivan, and D. J. Perreault, "A systematic approach to modeling impedances and current distribution in planar magnetics," *IEEE Transactions on Power Electronics*, vol. 31, no. 1, pp. 560–580, 2016.

[13] R. Prieto, R. Asensi, and J. A. Cobos, "Selection of the appropriate winding setup in planar inductors with parallel windings," in *2010 IEEE Energy Conversion Congress and Exposition*, 2010, pp. 4599–4604.

[14] W. Chen, Y. Yan, Y. Hu, and Q. Lu, "Model and design of pcb parallel winding for planar transformer," *IEEE Transactions on Magnetics*, vol. 39, no. 5, pp. 3202–3204, 2003.

[15] Y. Cai, "Optimal design of mhz llc converter for 48v bus converter application," Master's thesis, Virginia Tech, 8 2019.

[16] M. Li, Z. Ouyang, and M. A. Andersen, "Discovery of the nearly zero flux between two parallel conductors in planar transformers," *IEEE Transactions on Power Electronics*, vol. 37, no. 1, pp. 714–723, 2022.

[17] M. Solomentsev and A. J. Hanson, "Modeling current distribution within conductors and between parallel conductors in high frequency transformers," in *2021 IEEE Applied Power Electronics Conference and Exposition (APEC)*, 2021, pp. 1701–1708.

[18] J. Hu and C. Sullivan, "Ac resistance of planar power inductors and the quasidistributed gap technique," *IEEE Transactions on Power Electronics*, vol. 16, no. 4, pp. 558–567, 2001.

[19] A. J. Hanson and D. J. Perreault, "Modeling the magnetic behavior of n-winding components: Approaches for unshackling switching superheroes," *IEEE Power Electronics Magazine*, vol. 7, no. 1, pp. 35–45, 2020.

[20] M. Solomentsev, A. Bendapdui, and A. J. Hanson, "Quickshift: Rapid high-frequency transformer simulation and optimization," in *2022 IEEE 22nd Workshop on Control and Modeling for Power Electronics (COMPEL)*, 2022.